Published Online October 2022

Dept. of Mech. Engg.
CUET

Mechanical Engineering Research Journal
Vol. 12, pp. 19-29, 2020

ISSN: 1990-5491

# SYNTHESIS AND CHARACTERIZATION OF $TiO_2$ AND ZnO NANOPARTICLES

**U. D. Das, J. U. Ahamed, M. A. Mowazzem Hossain*, M. E. A. Razzaq, S. Dewanjee, and R. N. Jisu**

Department of Mechanical Engineering, Chittagong University of Engineering & Technology, Chattogram-4349, Bangladesh

**ABSTRACT**

In this experimental study, $TiO_2$ nanoparticles were synthesized using an ultrasound-assisted method, while the ZnO nanoparticles were fabricated using a chemical precipitation method. Results of X-ray diffraction indicate that the fabricated $TiO_2$ nanoparticles have a tetragonal anatase phase and ZnO nanoparticles have a hexagonal wurtzite phase. The calculated crystallite size of the fabricated nanoparticles using the Debye-Scherrer formula was consistent with the values estimated using the W-H plot and SSP methods. Crystallographic parameters of the XRD patterns were used to examine the dislocation density, morphology index, and specific surface area of the synthesized nanoparticles. The SEM images demonstrated uniform $TiO_2$ and ZnO nanostructures and suggest that both $TiO_2$ and ZnO nanoparticles were predominantly spherical in shape. The average grain size of 50.03 nm was observed for synthesized $TiO_2$ nanoparticles and 40.96 nm for ZnO nanoparticles.

***Keywords:*** *Nanoparticle synthesis, X-ray diffraction, SEM analysis, Williamson-Hall analysis, Size-Strain Plot.*

**NOMENCLATURE**

$\beta$ = Full width at half maximum (radian)
d = Interplanar Spacing ( $A^o$ )
K = Scherrer Constant (unitless)
$\lambda$ = X-ray wavelength (nm)
S = Specific surface area ($m^2/g$)
MI = Morphology Index (unitless)
D = Crystallite Size (nm)
$\rho$ = Density ($g\ cm^{-3}$)
$\delta$ = Dislocation Density ($m^{-2}$)
$\varepsilon$ = Strain (unitless)

## 1. INTRODUCTION

Nanoparticles are small particles ranging in diameter from 1 to 100 nm [1]. Due to their unique physical properties and material characteristics, nanoparticle synthesis is a promising research topic in a variety of areas, including engineering, material science, medicine, microbiology, environmental science, etc. [2].

Received : *02 January 2021*
Revised : *12 November 2021*
Accepted : *05 April 2022*

**Corresponding Author:*
E-mail: mowazzem@cuet.ac.bd

Chemically stable metals (e.g., gold, silver, nickel, copper), several allotropes of carbon (e.g., carbon nanotubes, diamond), metal oxides (e.g., alumina, silica, titania, zirconia), etc. are used as nanoparticles [3]. Metal oxide nanoparticles are relatively inexpensive and easy to synthesize. Two of the most commonly used metal oxide nanoparticles such as titanium dioxide ($TiO_2$) and zinc oxide (ZnO) are used in many applications [4].

Because of its high chemical stability, relatively low cost, and non-toxicity, $TiO_2$ is widely used as a photo-catalyst. It has also extensively been used in a variety of applications, including medicine, aerospace, photovoltaic equipment, paint, cosmetics, etc. [5]. According to Zallen et al. [6], $TiO_2$ exists primarily in three different forms: anatase, rutile, and brookite. The rutile and anatase forms have relatively more uses and both are widely investigated compared to brookite. Several studies show that rutile is more stable than anatase and brookites. Noted that both anatase and brookite convert into rutile form upon heating [7].

Zinc oxide nanoparticles are inexpensive, nontoxic, and safe metal oxides that are widely used in different applications. ZnO nanoparticles can be used in gas sensors, cosmetics, solar cells, luminescent materials, medicines, agricultural sectors, field- emission devices,

and so on, owing to their excellent chemical stability, wide direct band range (3.37 eV), and high exciton binding energy (60 meV) [8,9]. It can also be utilized as a polymer reinforcing agent, activator, and accelerator in place of micro-sized zinc oxide powder in the vulcanization of rubber materials to produce improved and more stable final products [8]. It has also become popular in foods, textiles, cosmetics, and food packaging, etc. due to its antifungal and antimicrobial properties [4].

To produce $TiO_2$ nanoparticles, many methods have been devised, including low-pressure gas evaporation, high-energy ball milling, plasma method, sol-gel, settling, hydrolysis, sputtering, spraying, and others [10]. There are also different ways of manufacturing ZnO nanoparticles, such as sol-gel, combustion synthesis, precipitation, spray pyrolysis, plasma synthesis, microemulsion, electroplating, chemical vapor deposition, pyrolysis, hydrothermal process, and so on [11,12]. Most of these methods are very expensive and are not suited to preparing large amounts of nanoparticles. $TiO_2$ nanoparticles were synthesized in this experiment using a modified sulfuric acid method with the use of ultrasound [10]. $TiO_2$ reagent powders (bulk powder) were chosen as a precursor, and the ultrasonic wave assisted in breaking down the chemical bonds in $TiO_2$ particles and initiating new structures by providing very intensive mixing and stirring up the reaction between $TiO_2$ powder and $H_2SO_4$. In the present study, ZnO nanoparticles were synthesized using the chemical precipitation method [11]. ZnO reagent powders (bulk powder) reacted with an ammonium hydrogen carbonate solution, leaving white ZnO and hydrozincite precipitates in the beaker at the end of the reaction. This hydrozincite completely changes into ZnO after drying and calcination. As a result, ZnO nanoparticles were effectively produced using ZnO reagent powder as a precursor. The two methods utilized here to produce $TiO_2$ and ZnO nanoparticles are easy, cost-effective, non-polluting, and convenient for large-scale production. Then, using XRD and SEM, the fabricated nanoparticles were characterized.

## 2. EXPERIMENTAL DETAILS

### 2.1 Materials

Extra-pure ZnO and $TiO_2$ powders were obtained from Taj Scientific, Chittagong, Bangladesh (manufactured by PT. Smart-Lab, Indonesia). Analytical grade $NH_4HCO_3$ was purchased from Jonaki Scientific Store, Dhaka, Bangladesh (manufactured by Loba Chemie Pvt. Ltd., India). The postgraduate lab of the Department of Physics, CUET, provided 98% $H_2SO_4$ and 25% $NH_4OH$ solution.

### 2.2 $TiO_2$ nanoparticle preparation

In this study, $TiO_2$ nanoparticle was prepared using an ultrasound-assisted method. First of all, 20 g of anatase titanium dioxide particles (reagent powder) was kept in a 500 ml beaker. Then, 40 ml of 98% sulfuric acid was added dropwise to the titanium dioxide particle in the beaker. The mixture was treated with ultrasound (40 kHz) for 45 mins in an ultrasonic bath. Then the beaker was transferred to an oven and heated at 100°C for 1 hour. The ultrasonic wave provides highly intensive mixing and stirs up the reaction between $TiO_2$ powder and $H_2SO_4$ [10]. As a result, at 100°C, the ultrasound assisted in breaking down the chemical bonds in $TiO_2$ particles and initiating new structures (Eq. 1). The beaker was then filled with distilled water, and the solution was stirred for five minutes with a glass rod. The pH was adjusted from 8 to 11 using a 25% ammonium hydroxide solution and filtered with filter paper to eliminate the by-products. Once filtering, the product was washed and filtered three more times. Subsequently, the sample was transferred to a separate beaker and dried at 30°C for 30 minutes in a water bath. Finally, the sample was annealed at 500°C for 2 hours. The whole process of synthesizing $TiO_2$ nanoparticles in this method is presented in a flowchart (Fig. 1) and a schematic diagram (Fig. 2). After calcination, the final product was well ground using mortar and pestle. The potential chemical processes during the interaction of $TiO_2$ with sulphuric acid are presented in the Eqs. (1)-(4) [10]:

$$TiO_2 + 2H_2SO_4 \xrightarrow[+\ 100\ ^oC]{\text{Ultrasonic energy}} H_2[TiO(SO_4)]F + H_2O \quad (1)$$

$$H_2[TiO(SO_4)_2] \longrightarrow TiOSO_4) + H_2SO_4 \quad (2)$$

$$TiOSO_4 + (n+1)H_2O \longrightarrow TiO_2\ nH_2O + H_2SO_4 \quad (3)$$

$$TiO_2\ nH_2O \longrightarrow TiO_2 + nH_2O \quad (4)$$

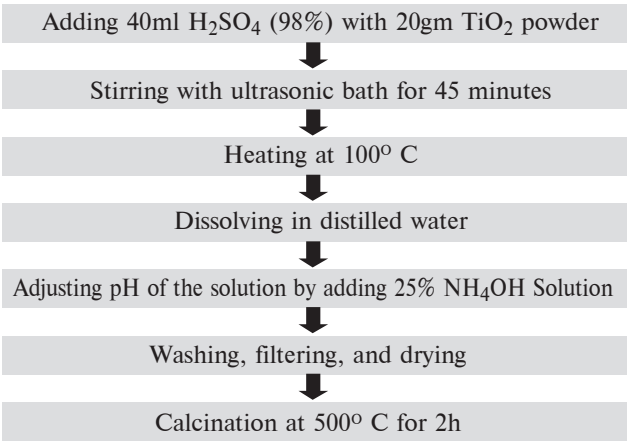


***Fig. 1 A flowchart of the fabrication process of $TiO_2$ nanoparticles using the modified sulfuric acid method with the aid of ultrasound.***

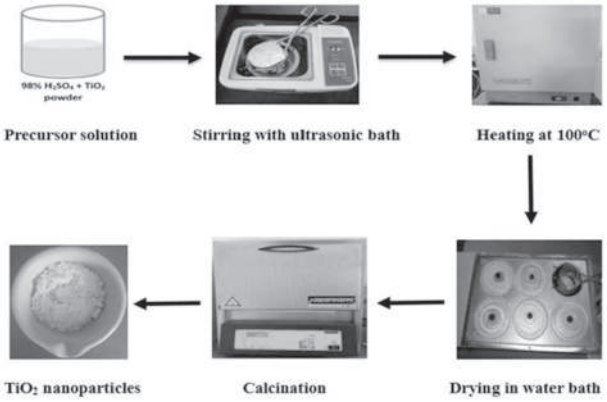


*Fig. 2 Schematic representation of $TiO_2$ nanoparticles synthesis process.*

## 2.3 ZnO nanoparticle preparation

At first, 120 ml of distilled water was taken in a 500 ml beaker and 96 gm of ammonium bicarbonate was dissolved in the distilled water. Then, 16 gm of ZnO powder was added to the prepared $NH_4HCO_3$ solution and stirred for 5-6 minutes with a glass rod to completely dissolve ZnO in the solution. The beaker was then placed on the hot plate stirrer (magnetic stirrer with hot plate) and 32 gm of ZnO powder was added into the solution under stirring at 60°C. After two hours, the beaker was put down from the hot plate stirrer and white precipitates were dried in a water bath at about 70°C for 10 hours. The resulting mixture was then calcined at 400°C for about 1 hour 30 mins. The whole process of synthesizing ZnO nanoparticles is presented in a flowchart (Fig. 3) and a schematic diagram (Fig. 4). After calcination, the final product was well ground using mortar and pestle. In Fig. 4, a schematic diagram represents the steps of the nanoparticle synthesis process. The reactions occurring in the ZnO nanoparticle formation are shown in the Eqs. (5) - (8) [11]:

$$NH_4HCO_3 + H_2O \longrightarrow NH_4^+ + HCO_3^- + NH_3 + CO_3^{2-} + OH^- \quad (5)$$

$$NH_4^+ + HCO_3^- + NH_3 + CO_3^{2-} + OH^- \longleftrightarrow$$

$$\underbrace{NH_3; NH_4OH; (NH_4)_2CO_3; NH_4HCO_3; H_2O}_{\textbf{AHCH (Ammonium hydrogen carbonate solution)}} \quad (6)$$

$$ZnO + AHCH \longrightarrow ZnO\downarrow + xNH_3\uparrow + yH_2O\uparrow + zCO_2\uparrow + Zn_5(OH)_6(CO_3)_2\downarrow \quad (7)$$

The XRD data reveal that, after calcination at 400°C, the precipitated hydrozincite ($Zn_5(OH)_6(CO_3)_2$) entirely transforms to zinc oxide.

$$Zn_5(OH)_6(CO_3)_2 \longrightarrow 5ZnO + 2CO_2 + 3H_2O \quad (8)$$

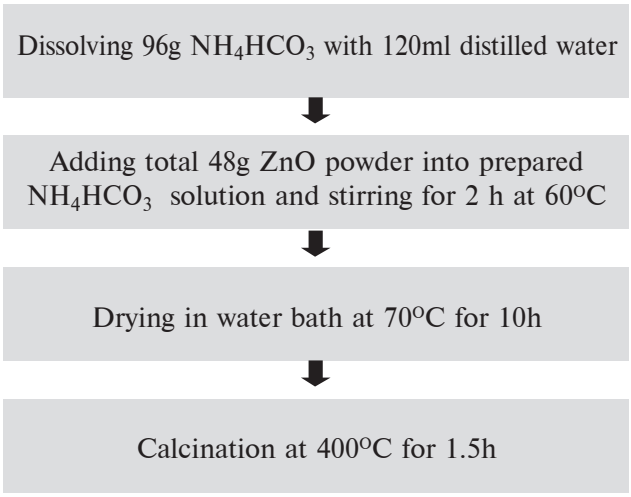


*Fig. 3 A flowchart of the preparation process of ZnO nanoparticles using the chemical precipitation method.*

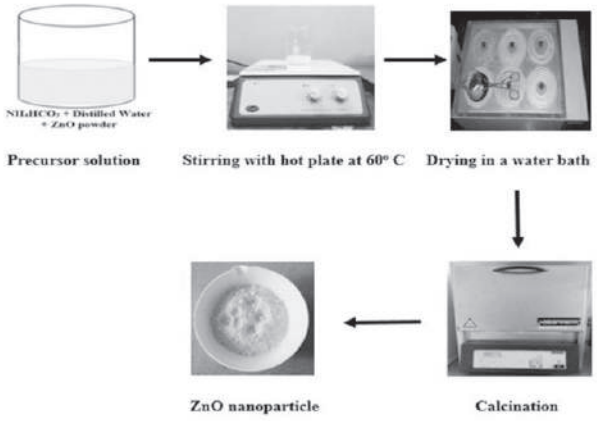


*Fig. 4 Schematic representation of ZnO nanoparticles synthesis process.*

## 2.4 Characterization

In this experimental study, the crystal structure and microstructure of the fabricated $TiO_2$ and ZnO nanoparticles were analyzed using XRD (GBC scientific; $Cu\_K_{\alpha 1}$: $\lambda$ = 1.54062A° radiation source) and SEM (model: JSM 7600F, JEOL-Japan). XRD data were used to examine the crystallite size, morphology index, dislocation density, and specific surface area.

## 3. RESULTS AND DISCUSSION

### 3.1 XRD analysis

Table 1 presents the crystallographic parameters of the XRD pattern of the fabricated $TiO_2$ nanoparticles, which is graphically illustrated in Fig. 5. In Fig. 5, the XRD pattern of the $TiO_2$ nanoparticle was consistent with JCPDS data (PDF No: 21-1272) and previously reported data [5,13]. The presence of peaks at 2θ values of 25.4, 37.04, 37.9, 38.67, 48.15, 53.99, 55.16, 62.78, 68.84,

and 70.36° corresponding to <101>, <103>, <004>, <112>, <200>, <105>, <211>, <204>, <116> and <220> lattice planes were observed. The strong peaks at 25.4° and 48.15° suggest that the synthesized $TiO_2$ nanoparticle was in the anatase phase [5,13].

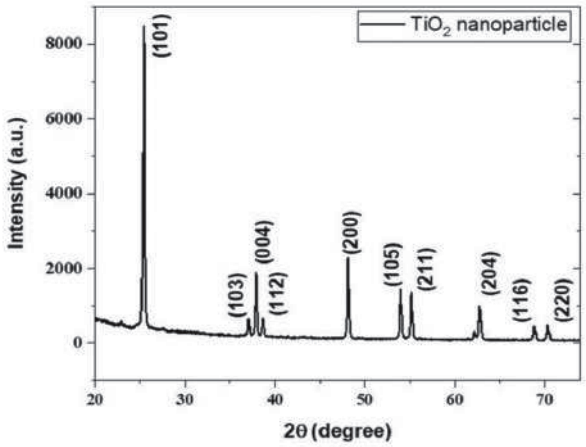


*Fig. 5 X-ray diffraction pattern of the synthesized $TiO_2$ nanoparticles.*

The crystal system of synthesized anatase $TiO_2$ nanoparticles was tetragonal-body centered. Miller indices <*hkl*> and d spacing were used to estimate the lattice parameters (a=b, c) and unit cell volume (V) of $TiO_2$ using the following relations [14]:

$$\frac{1}{d^2} = \frac{h^2 + k^2}{a^2} + \frac{1^2}{c^2} \tag{9}$$

$$V = a^2 c \tag{10}$$

The a, b, c and V of the fabricated $TiO_2$ nanoparticles can be calculated for the plane <004> and <101> and tabulated in Table 2. The obtained lattice parameters and unit cell volume of the $TiO_2$ nanoparticles were highly agreed with the previous experimental results of the anatase $TiO_2$, as shown in Table 2. Table 3 presents the crystallographic parameters of the XRD pattern of the fabricated ZnO nanoparticles, which is graphically illustrated in Fig. 6. The XRD pattern of the synthesized ZnO nanoparticle was consistent with JCPDS data (JCPDS Card No.: 01-089-0510) and previously reported data. The characteristic peaks of the hexagonal zinc oxide wurtzite were examined at 2θ values of 31.8, 34.44, 36.26, 47.54, 56.62, 62.86, 66.4, 67.94, 69.06, and 72.56° which were generated by the reflections from <100>, <002>, <101>, <102>, <110>, <103>, <200>, <112>, <201> and <004> lattice planes.

The sharp and narrow peak intensity confirms that the synthesized ZnO nanoparticle is high quality with fine grain size and good crystallinity.

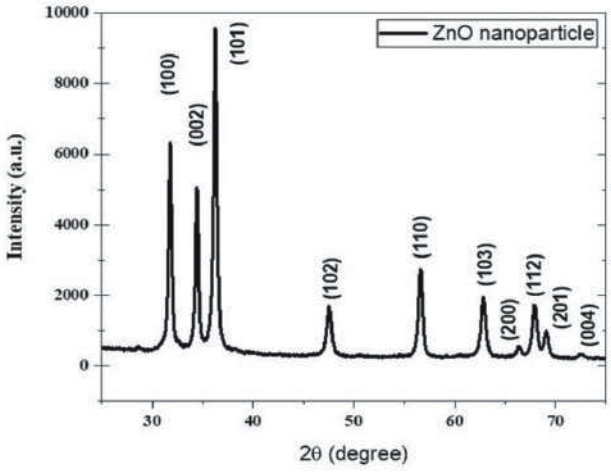


*Fig. 6 X-ray diffraction pattern of the fabricated ZnO nanoparticles.*

As the crystal structure of the synthesized ZnO nanoparticle is hexagonal wurtzite, the lattice parameters have been computed using Miller indices <*hkl*> and d spacing according to the following relations

$$\frac{1}{d_{hkl}^2} = \frac{4}{3}\left(\frac{h^2 + hk + k^2}{a^2}\right) + \frac{l^2}{c^2} \tag{11}$$

With the first-order approximation, n = 1;

$$\sin^2\theta = \frac{\lambda^2}{4a^2}\left[\frac{4}{3}(h^2 + k^2 + hk + \left(\frac{a}{c}\right)^2 l^2\right] \tag{12}$$

The lattice constant 'a' for <100> plane is calculated by

$$a = \frac{\lambda}{\sqrt{3}\sin\theta} \tag{13}$$

For the plane <002>, the lattice constant 'c' is estimated by

$$C = \frac{\lambda}{\sin\theta} \tag{14}$$

The unit cell volume of the fabricated ZnO nanoparticles can be

$$V = \frac{\sqrt{3}\,a^2 c}{2} \tag{15}$$

here, λ is the X-ray wavelength (0.154062 nm). The obtained parameters of the synthesized ZnO nanoparticles are presented in Table 4. The synthesized ZnO nanoparticles values are in good agreement with the previously reported experimental data of hexagonal wurtzite ZnO.

## 3.2 Crystallite size analysis

### 3.2.1 Scherrer Method

The crystallite size of the particles in this study was evaluated using the Debye-Scherrer formula.

$$D = \frac{k\,\lambda}{\beta\,cos\,\theta} \tag{16}$$

The inter-planar spacing between atoms (d-spacing) can be obtained using Bragg's Law (Eq. (17).

$$2d\sin\theta = n\lambda \tag{17}$$

here, D is the crystallite size, λ is the X-ray wavelength (0.154062 nm), k is the Scherrer constant (0.89), β is FWHM (full width at half maximum), θ is diffraction angle, and d is interplanar spacing. The Scherrer formula was used to calculate the average crystallite size of the fabricated $TiO_2$ and ZnO nanoparticles from the XRD peak width of <101>, which are tabulated in Table 5 along with other geometrical parameters. The surface area per unit mass is specified as the specific surface area (SSA). It is a material property that is used to determine a material's type and properties. When the size of the materials is decreased, the specific surface area increases. The specific surface area is estimated using Eq. (18) [15]:

$$S = \frac{6 \times 10^3}{D \times \rho} \tag{18}$$

In this equation, D denotes particle size (crystallite size) and ρ represents the density of synthesized nanoparticles. The density of anatase $TiO_2$ is 3.894 g/cm$^3$ [16] and ZnO is 5.606 g/cm$^3$ [15]. The length of dislocation lines per unit volume of the crystal is defined as the dislocation density [17]. The dislocation density decreases while the grain size increases. A dislocation is a crystallographic deformity, or disorderliness, where the atoms are out of position in the crystal structure. It is commonly acknowledged that the presence of dislocations causes material characteristics to change. The dislocation density can be calculated using Eq. (19):

$$\delta = \frac{1}{D^2} \tag{19}$$

***Table 1 Crystallographic parameters of the XRD pattern and structural parameters related to the synthesized $TiO_2$ nanoparticles***

| Plane (*hkl*) | 2θ | FWHM (radian) | Crystallite Size (nm) | Interplanar Spacing (A°) | Morphology Index (unitless) | Specific Surface Area ($m^2/g$) | Dislocation Density ($m^{-2}$) |
|---|---|---|---|---|---|---|---|
| 101 | 25.4 | 0.003508 | 40.07 | 3.50 | .619 | 38.45 | $6.23\times 10^{14}$ |
| 103 | 37.04 | 0.003543 | 40.82 | 2.42 | .617 | 37.74 | $6.00\times 10^{14}$ |
| 004 | 37.9 | 0.004076 | 35.56 | 2.37 | .583 | 43.31 | $7.91\times 10^{14}$ |
| 112 | 38.67 | 0.005201 | 27.94 | 2.33 | .523 | 55.14 | $12.8\times 10^{14}$ |
| 200 | 48.15 | 0.004016 | 37.40 | 1.89 | .587 | 41.19 | $7.15\times 10^{14}$ |
| 105 | 53.99 | 0.004251 | 36.20 | 1.697 | .573 | 42.55 | $7.63\times 10^{14}$ |
| 211 | 55.16 | 0.004363 | 35.45 | 1.66 | .567 | 43.45 | $7.96\times 10^{14}$ |
| 204 | 62.78 | 0.005204 | 30.87 | 1.48 | .523 | 49.91 | $10.49\times 10^{14}$ |
| 116 | 68.84 | 0.00548 | 30.83 | 1.36 | .510 | 50.79 | $10.87\times 10^{14}$ |
| 220 | 70.36 | 0.005707 | 29.39 | 1.34 | .499 | 52.41 | $11.57\times 10^{14}$ |

***Table 2 The lattice parameters and unit cell volume of the synthesized $TiO_2$ nanoparticles and their differences with the experimental measurements***

| Sample | a (nm) | c (nm) | V (nm$^3$) |
|---|---|---|---|
| Synthesized | 0.377 | 0.9488 | 0.1349 |
| Experimental [16] | 0.3785 | 0.9514 | 0.1363 |
| Deviation (%) | 0.396% | 0.273% | 1.02% |

***Table 4 The lattice parameters and unit cell volume of the synthesized ZnO nanoparticles and their differences with the previous experimental measurements***

| Sample | a (nm) | c (nm) | V ($nm^3$) |
|---|---|---|---|
| Synthesized ZnO | 0.3247 | 0.5204 | 0.04752 |
| Experimental [15] | 0.3254 | 0.5215 | 0.04782 |
| Deviation(%) | 0.154% | 0.211% | 0.627% |

***Table 3 Crystallographic parameters of the XRD pattern and structural parameters related to the synthesized ZnO nanoparticles***

| Plane (*hkl*) | 2$\theta$ (degree) | FWHM (radian) | Crystallite Size (nm) | Interplanar Spacing (A°) | Morphology Index | Specific Surface Area ($m^2/g$) | Dislocation Density ($m^{-2}$) |
|---|---|---|---|---|---|---|---|
| 100 | 31.8 | 0.00642 | 22.15 | 2.81 | .620 | 47.74 | $1.985 \times 10^{15}$ |
| 002 | 34.44 | 0.00611 | 23.74 | 2.60 | .631 | 45.12 | $1.773 \times 10^{15}$ |
| 101 | 36.26 | 0.00735 | 19.85 | 2.48 | .587 | 53.97 | $2.538 \times 10^{15}$ |
| 102 | 47.54 | 0.00936 | 16.20 | 1.91 | .528 | 66.16 | $3.813 \times 10^{15}$ |
| 110 | 56.62 | 0.00955 | 16.48 | 1.62 | .523 | 64.97 | $3.678 \times 10^{15}$ |
| 103 | 62.86 | 0.00881 | 18.45 | 1.48 | .543 | 58.08 | $2.939 \times 10^{15}$ |
| 200 | 66.4 | 0.00766 | 21.63 | 1.41 | .577 | 49.54 | $2.138 \times 10^{15}$ |
| 112 | 67.94 | 0.00895 | 16.56 | 1.38 | .509 | 64.68 | $3.645 \times 10^{15}$ |
| 201 | 69.06 | 0.00895 | 18.79 | 1.36 | .539 | 56.998 | $2.830 \times 10^{15}$ |
| 004 | 72.56 | 0.01046 | 16.43 | 1.30 | .500 | 65.02 | $3.703 \times 10^{15}$ |

On the other hand, the morphology index (MI) can be obtained using the following relation:

$$MI = \frac{FWHM_h}{FWHM_h + FWHM_p} \tag{20}$$

where $FWHM_h$ is the *FWHM* of the particular peak for which the morphology index is being studied, and $FWHM_h$ is the greatest *FWHM* value derived from the peaks.

The structural parameters like morphology index, dislocation density, and specific surface area (SSA) in different lattice planes are calculated for both $TiO_2$ and ZnO nanoparticles and presented in Tables 1 and 2 respectively. Figures 7(a) and 7(b) illustrate the dislocation density vs. crystallite size graph for synthesized $TiO_2$ and ZnO nanoparticles, respectively. It can be seen in Figs. 7(a) and 7(b) that the dislocation density is reversed to the particle size of the material. Hence, synthesized nanoparticles are stronger and harder than their bulk counterparts [13]. The morphology index is directly proportional to particle size and in reverse to the specific surface area, as shown in Figs. 8 and 9.

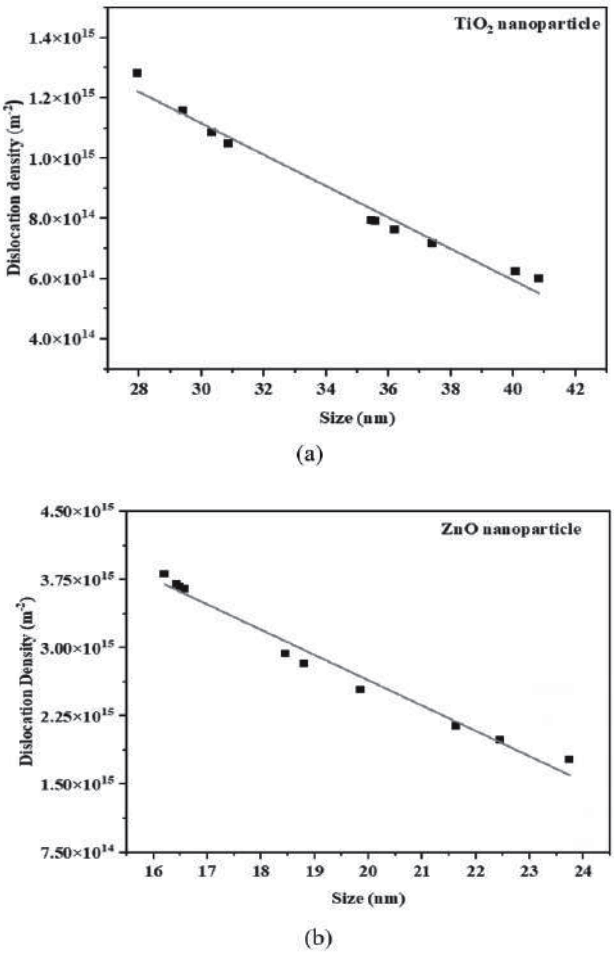


***Fig. 7 Plot of dislocation density vs crystallite size for - a) $TiO_2$ nanoparticles and b) ZnO nanoparticles.***

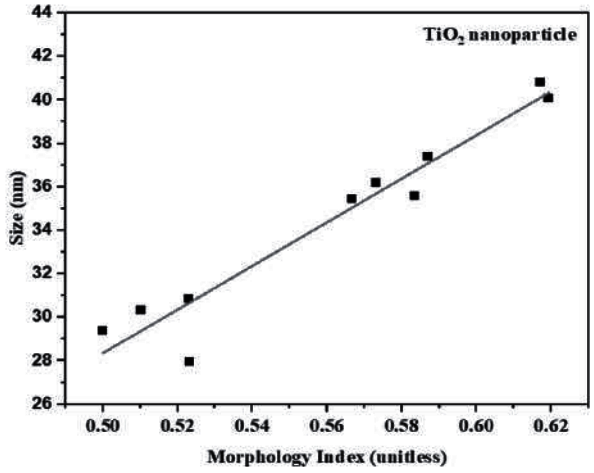


(a)

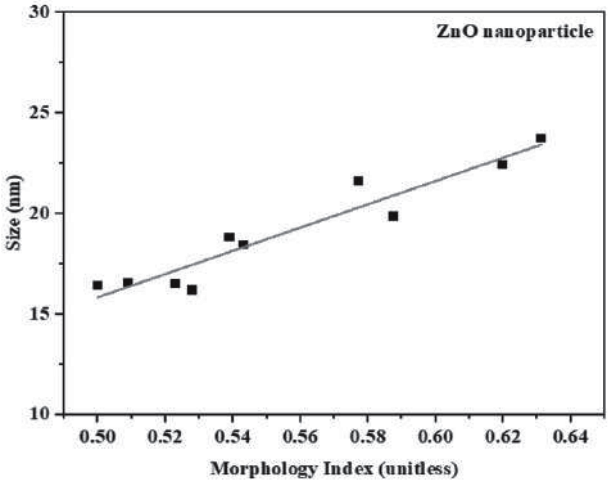


(b)

*Fig. 8 Plot of crystallite size vs morphology index for - a) $TiO_2$ nanoparticles and b) ZnO nanoparticles.*

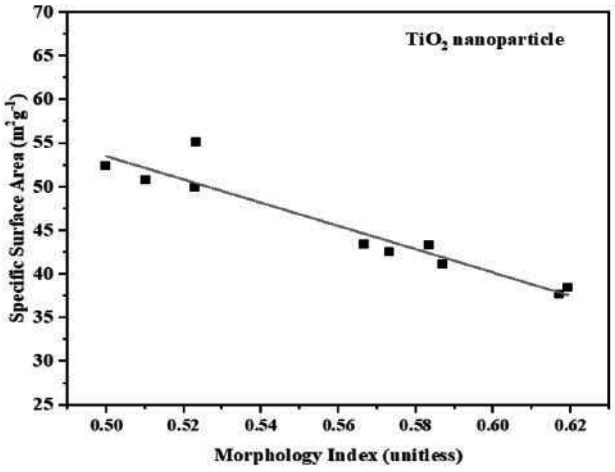


(a)

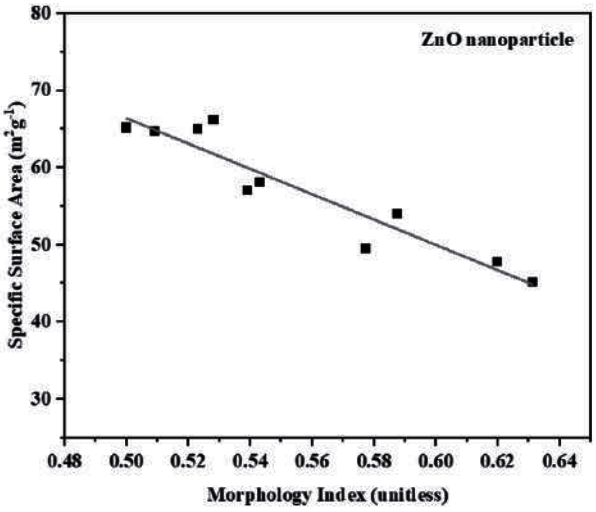


(b)

*Fig. 9 Plot of specific surface area vs morphology index for - a) $TiO_2$ nanoparticles and b) ZnO nanoparticles.*

### 3.2.2 Williamson-Hall method

A perfect crystal is one in which all atoms are in their ideal position and has no imperfections. Finite crystal size and its associated lattice strain, according to Williamson-Hall, are the departures from perfect crystal [14]. The strain induced by distortion and crystal imperfection in powders can be estimated as follows:

$$\varepsilon = \frac{\beta}{4sin\,\theta} \tag{21}$$

Now, the total peak broadening can be written

$$B_{hkl} = \beta_D + \beta_\varepsilon \tag{22}$$

where $\beta_D$ is the broadening due to the contribution of crystallite size, $\beta_\varepsilon$ is the broadening due to strain.

Assuming that the particle size and strain contributions to line broadening are independent and have a profile Cauchy-like, the observed line breadth is commonly written as [18]

$$\beta = \frac{k\,\lambda}{Dcos\,\theta} + 4\,\varepsilon\,\tan\theta \tag{23}$$

Rearranging Eq. (23), we get

$$\beta\cos\theta = \frac{k\lambda}{D} + 4\,\varepsilon\,\sin\theta \tag{24}$$

The above equation is called the Williamson−Hall equation, and it is also referred to as the Uniform Deformation Model (UDM). Here, the crystal is assumed to be isotropic and the material properties are supposed to be independent of crystallographic directions [8]. In Figs. 10(a) and 10(b), the positive slopes and non-zero y-intercepts indicate that they were isotropic in nature. The crystallite size and strain value derived by the 'W-H' method are tabulated in Table 5.

### 3.2.3 Size-strain plot method (SSP)

The 'Size−Strain Plot' (SSP) method can also be used to obtain the size−strain parameters. When the strain profile is stated by a Gaussian function and the crystallite size is described by a Lorentzian function, it allows for a better estimation of size-strain parameters [8,9].

$$(d_{hkl}\,\beta_{hkl}\cos\theta_{hkl})^2 = \frac{1}{V_s}\,(d^2_{hkl}\,\beta_{hkl}\cos\theta_{hkl}) + (\frac{\varepsilon_a}{2})^2 \qquad (25)$$

where $d_{hkl}$ denotes interplanar lattice spacing, $\varepsilon a$ denotes the apparent strain, and $Vs$ denotes apparent volume-weighted average size. In Figs. 11(a) and 11(b) two plots are drawn taking $(d_{hkl}\beta_{hkl}\cos\theta_{hkl})^2$ in the y axis and $d^2_{hkl}\beta_{hkl}\cos\theta_{hkl}$ on the x-axis for synthesized $TiO_2$ and ZnO nanoparticles respectively. For spherical crystallites, the crystallite size can be determined by [8]

$$D_s = \frac{4}{3} V_s \qquad (26)$$

As a result, the slope of the linear fit may be used to determine crystallite size, and the y-intercept can be used to estimate strain value. Table 5 presents the crystallite size and strain value derived using the 'Size-Strain Plot' method.

***Table 5: Geometrical parameters of the synthesized $TiO_2$ and ZnO nanoparticles***

| Sample | Scherrer Method | Williamson-Hall plot (UDM) | | Size-strain plot | |
|---|---|---|---|---|---|
| | $D_{avg}$(nm) | D (nm) | ε (no unit) | D (nm) | ε (no unit) |
| $TiO_2$ | 40.07 | 46.3 | 0.000654 | 37.9 | 0.0054 |
| ZnO | 19.85 | 26.02 | 0.00118 | 22.71 | 0.0115 |

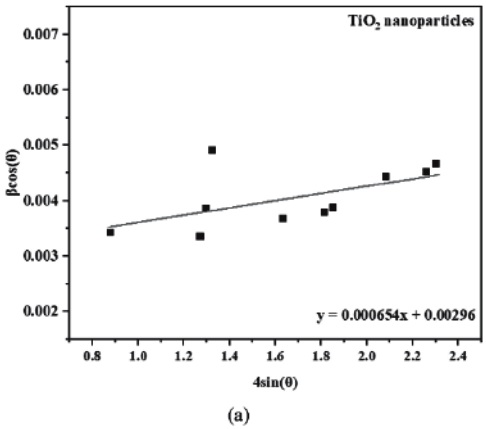


(a)

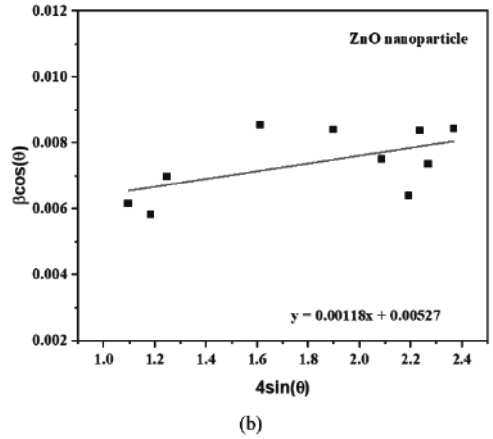


(b)

***Fig. 10 Williamson-Hall plot for - a) TiO2 nanoparticles and b) ZnO nanoparticles.***

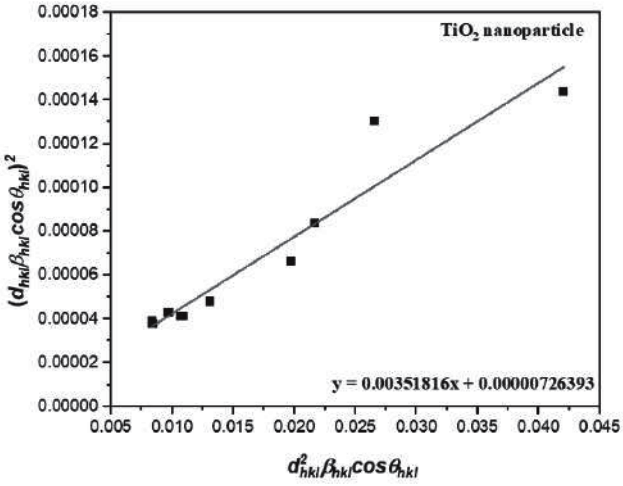


(a)

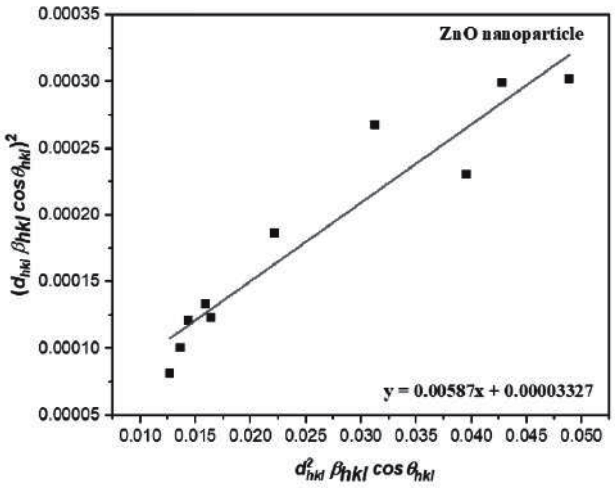


(b)

***Fig. 11 The Size-Strain Plot (SSP) for - a) $TiO_2$ nanoparticles and b) ZnO nanoparticles.***

### 3.2.4 Estimation of RMS strain

The following relationships were used to determine the maximum or upper limit microstrain and the root mean square (RMS) microstrain along with the crystallographic directions [8,20]

$$\varepsilon_{hkl} = \left(\frac{\Delta d_{hkl}}{d_{o\,hkl}}\right) \quad (27)$$

and

$$< \varepsilon_{rms} >= \left(\frac{2}{\pi}\right)^{\frac{1}{2}} \varepsilon_{hkl} \quad (28)$$

where $d_{ohkl}$ and $d_{hkl}$ represent the ideal and observed interplanar spacing values, respectively. In Figs. 12(a) and 12(b) two plots are drawn taking $\varepsilon_{hkl}$ values on the x-axis and corresponding $\varepsilon rms$ values on the y-axis for synthesized $TiO_2$ and ZnO nanoparticles respectively. When the strain values are in good agreement, the points should be on a straight line with a $45^0$ angle to the x-axis. Here, $\varepsilon_{rms}$ for both the nanoparticles vary linearly with the values of $\varepsilon_{hkl}$. This implies that no incongruity exists between the measured and ideal interplanar spacing values of the synthesized nanoparticles [14].

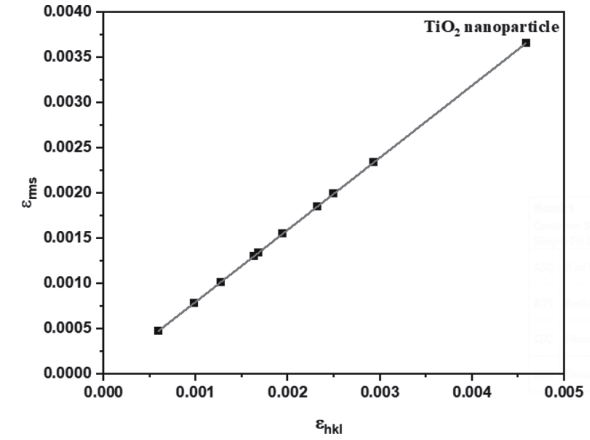


(a)

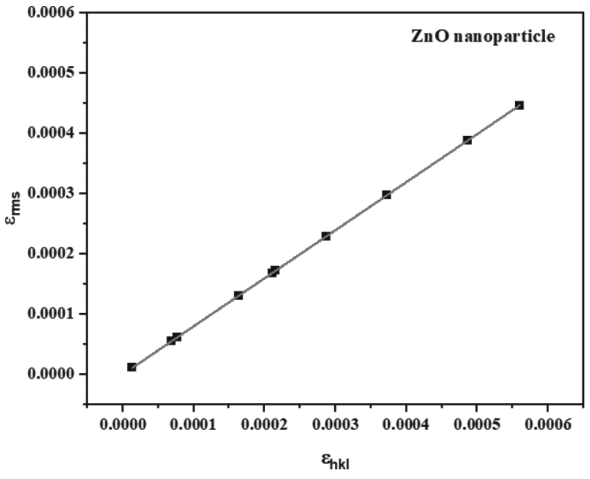


(b)

***Fig. 12 Plot of $\varepsilon_{rms}$ vs $\varepsilon_{hkl}$ for - a) $TiO_2$ nanoparticles and b) ZnO nanoparticles.***

### 3.3 SEM analysis

The shape and morphology of nanoparticles are observed in the FESEM micrograph as shown in Figs. 13 and 15, respectively. The SEM images in Figs. 13(a) and 13(b) demonstrate a uniform structure and size for $TiO_2$ nanoparticles. The fabricated $TiO_2$ nanoparticles are predominantly spherical in shape. However, some moderately agglomerated particles and elongated particles are also observed in the SEM images. The average grain size of $TiO_2$ nanoparticles is about 50.03 nm (using ImageJ software). ZnO nanoparticles are mostly spherical in shape as well, as can be seen in Figs. 15(a) and 15(b), with an average grain size of approximately 40.96 nm. There was also a small amount of agglomeration in the synthesized ZnO nanoparticles. The grain size distributions of the synthesized nanoparticles are shown in Figs. 14 and 16.

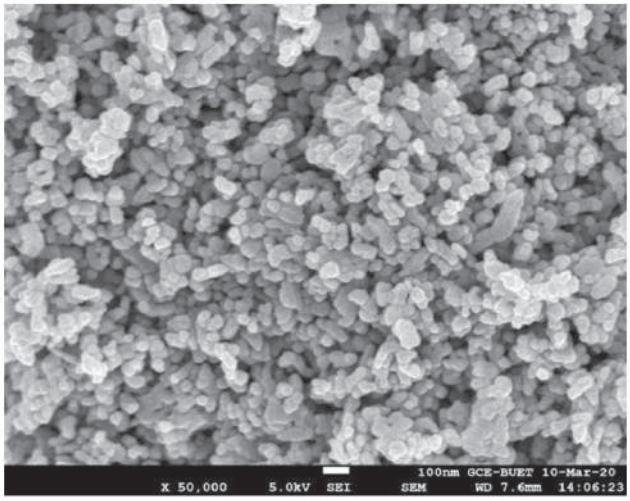


(a)

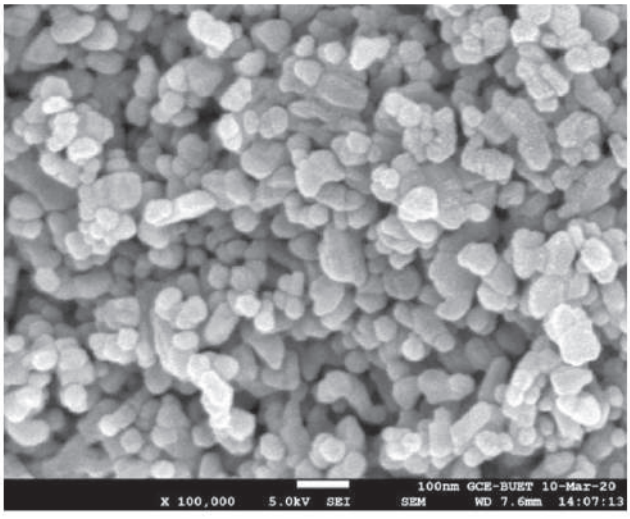


(b)

***Fig. 13 SEM Image of the Synthesized $TiO_2$ Nanoparticles (a) 50,000 magnification and (b) 100,000 magnification.***

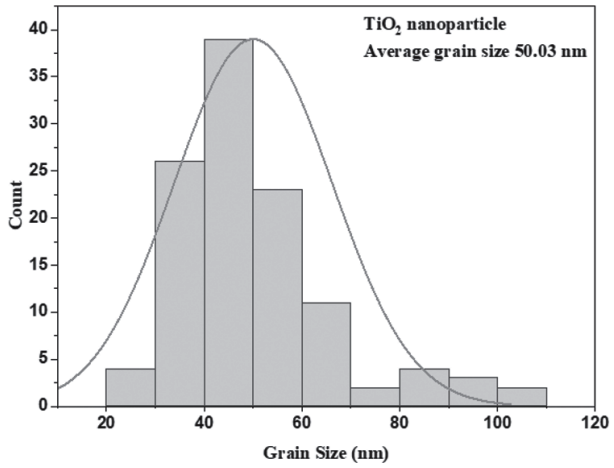


*Fig. 14 Grain size distribution of the fabricated $TiO_2$ nanoparticles.*

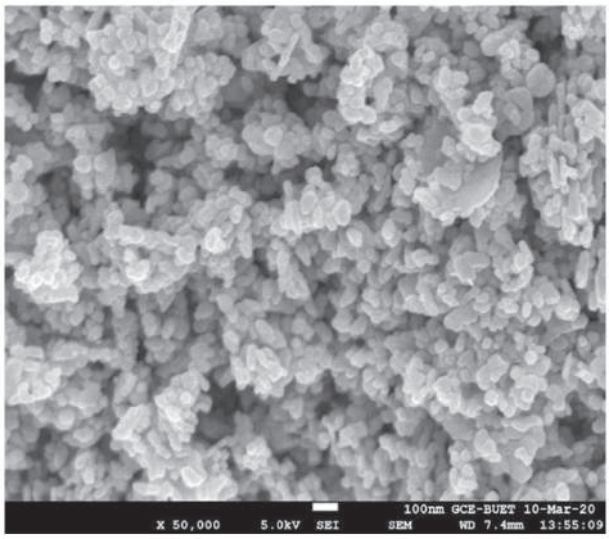


(a)

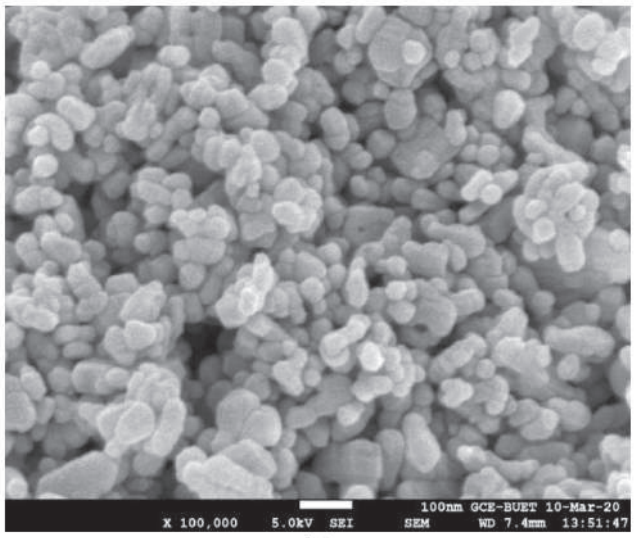


(b)

*Fig. 15 SEM Image of the Synthesized ZnO Nanoparticles (a) 50,000 magnification and (b) 100,000 magnification.*

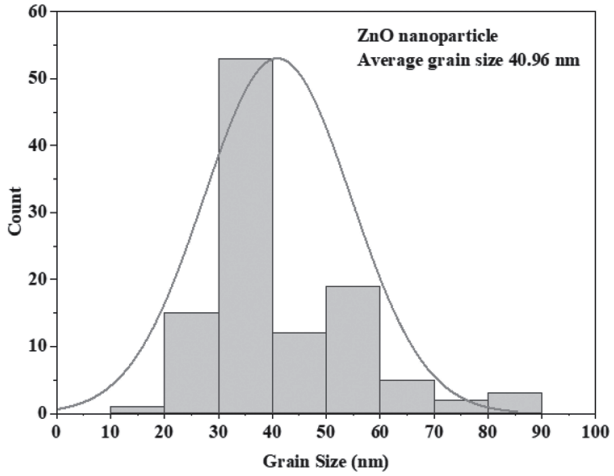


*Fig. 16 Grain size distribution of the synthesized ZnO nanoparticles.*

## 4. CONCLUSIONS

$TiO_2$ nanoparticles have been successfully synthesized with the aid of ultrasound using the sulfuric acid method, and ZnO nanoparticles were fabricated using a chemical precipitation method. The XRD analysis has affirmed that the fabricated $TiO_2$ nanoparticles are tetragonal anatase phase, while the ZnO nanoparticles have hexagonal wurtzite structure. The crystallite size of the fabricated nanoparticles determined using the Scherrer formula are agreed well with the W-H and SSP method values. Both the W-H and SSP methods estimate the lattice strain ε, and they are agreed well. The SEM images demonstrate uniform ZnO and $TiO_2$ nanostructures. The average grain size of 50.03 nm was observed for synthesized $TiO_2$ nanoparticles and 40.96 nm for ZnO nanoparticles.

## 5. ACKNOWLEDGEMENT

This experimental investigation was conducted in the postgraduate lab of the Department of Physics, CUET. The authors are thankful to Prof. Dr. Md. Mohi Uddin (Department of Physics, CUET) for his co-operations. The authors also gratefully thank to the Solar Energy Technology Research Laboratory of IFRD in BCSIR, Dhaka and Electron Microscopy Laboratory in the Department of Glass and Ceramic Engineering (GCE), BUET.

## REFERENCES


[1] I. Khan, K. Saeed, and I. Khan, "Nanoparticles: Properties, applications and toxicities," Arabian Journal of Chemistry, vol. 12, no. 7. Elsevier B.V., pp. 908−931, Nov. 01, 2019, doi: 10.1016/j.arabjc.2017.05.011.

[2] P. Dobson, J. Helen, and S. King, "Nanoparticle," May 14, 2019. https://www. britannica.com/ science/nanoparticle (accessed Dec. 30, 2020).

[3] H. Kim, "Enhancement of critical heat flux in nucleate boiling of nanofluids: A state-of-art review," Nanoscale Research Letters, vol. 6. pp. 1−18, 2011, doi: 10.1186/1556-276X-6-415.

[4] I. de Angelis et al., "Comparative study of ZnO and $TiO_2$ nanoparticles: Physicochemical characterisation and toxicological effects on human colon carcinoma cells," Nanotoxicology, vol. 7, no. 8, pp. 1361−1372, 2013, doi: 10.3109/17435390.2 012.741724.

[5] T. Thirugnanasambandan, T. Theivasanthi, and M. Alagar, "Titanium dioxide ($TiO_2$) Nanoparticles XRD Analyses: An Insight Titanium dioxide ($TiO_2$) Nanoparticles-XRD Analyses-An Insight." [Online]. Available: https://www.researchgate.net/ publication/244990066.

[6] R. Zallen and M. P. Moret, "The optical absorption edge of brookite $TiO_2$," Solid State Communications, vol. 137, no. 3, pp. 154−157, Jan. 2006, doi: 10.1016/j.ssc.2005.10.024.

[7] P. Nyamukamba, O. Okoh, H. Mungondori, R. Taziwa, and S. Zinya, "Synthetic Methods for Titanium Dioxide Nanoparticles: A Review," in Titanium Dioxide - Material for a Sustainable Environment, InTech, 2018.

[8] P. Bindu and S. Thomas, "Estimation of lattice strain in ZnO nanoparticles: X-ray peak profile analysis," Journal of Theoretical and Applied Physics, vol. 8, no. 4, pp. 123− 134, Dec. 2014, doi: 10.1007/s40094-014-0141-9.

[9] Y. Zhang, M. K. Ram, E. K. Stefanakos, and D. Y. Goswami, "Synthesis, characterization, and applications of ZnO nanowires," Journal of Nanomaterials, vol. 2012. 2012, doi: 10.1155/ 2012/624520.

[10] N. T. Duong, L. D. Vuong, N. M. Son, H. van Tuyen, and T. van Chuong, " The synthesis of $TiO_2$ nanoparticles using sulfuric acid method with the aid of ultrasound ," Nanomaterials and Energy, vol. 6, no. 2, pp. 82−88, Dec. 2017, doi: 10.1680/jnaen.17.00009.

[11] Z. M. Khoshhesab, M. Sarfaraz, and M. A. Asadabad, "Preparation of ZnO nanostructures by chemical precipitation method," Synthesis and Reactivity in Inorganic, Metal-Organic and Nano-Metal Chemistry, vol. 41, no. 7, pp. 814−819, Aug. 2011, doi: 10.1080/ 15533174.2011.591308.

[12] S. Talam, S. R. Karumuri, and N. Gunnam, "Synthesis, Characterization, and Spectroscopic Properties of ZnO Nanoparticles," ISRN Nanotechnology, vol. 2012, pp. 1− 6, 2012, doi: 10.5402/2012/372505.

[13] M. I. Pratheepa and M. Lawrence, "X-Ray Diffraction Analyses of Titanium Dioxide Nanoparticles," International Journal of Scientific Research in Science and Technology, 2017, [Online]. Available: https://www. researchgate.net/ publication/331588449.

[14] R. V. Vijayalakshmi, S. Selvarani, P. Praveen Kumar, P. Rajakumar, and K. Ravichandran, "Investigations on structural and optical properties of chalcone dendrimer in $Ag@TiO_2$ core−shell nanoparticles," Applied Physics A: Materials Science and Processing, vol. 124, no. 11, Nov. 2018, doi: 10.1007/s00339-018-2177-1.

[15] D. Pinjari, "Ultrasound assisted green synthesis of zinc oxide nanorods at room temperature Metal Organic Framework View project Doctoral Research Work View project," 2016. [Online]. Available: https://www.researchgate.net/ publication/ 303682162.

[16] D. Hanaor, C. Sorrell, D. A. H. Hanaor, and C. C. Sorrell, "Review of the anatase to rutile phase transformation," Journal of Ma-terials Science, vol. 46, no. 4, 2011, doi: 10.1007/s10853-010-5113-0п.

[17] L. C. Nehru, V. Swaminathan, and C. Sanjeeviraja, "Photoluminescence Studies on Nanocrystalline Tin Oxide Powder for Optoelectronic Devices," American Journal of Materials Science, vol. 2, no. 2, pp. 6−10, Aug. 2012, doi: 10.5923/ j.materials. 20120202.02.

[18] V. D. Mote, Y. Purushotham, and B. N. Dole, "Williamson-Hall analysis in estimation of lattice strain in nanometer-sized ZnO particles,"2012. [Online]. Available:http://www.jtaphys.com/ content/ 2251-7235/6/1/6.

[19] M. A. Tagliente and M. Massaro, "Strain-driven (0 0 2) preferred orientation of ZnO nanoparticles in ion-implanted silica," Nuclear Instruments and Methods in Physics Research, Section B: Beam Interactions with Materials and Atoms, vol. 266, no. 7, pp. 1055−1061, Apr. 2008, doi: 10.1016/ j.nimb.2008.02.036.

[20] A.J.C. Wilson, "X-ray optics: The diffraction of X-rays by finite and imperfect crystals", 2nd Edition, London, Methuen, 1962.